Ultrasound in Med. & Biol., Vol. 27, No. 6, pp. 829–839, 2001

0301-5629/01/$–see front matter

ELSEVIER

PII: S0301-5629(01)00375-1

● *Original Contribution*

TEMPORAL AND SPATIAL EVALUATION OF LESION REPARATIVE RESPONSES FOLLOWING SUPERTHRESHOLD EXPOSURE OF RAT LUNG TO PULSED ULTRASOUND

JAMES F. ZACHARY,* LEON A. FRIZZELL,† KANDICE S. NORRELL,* JAMES P. BLUE, JR,* RITA J. MILLER† and WILLIAM D. O'BRIEN, JR†

*Department of Veterinary Pathobiology; and †Bioacoustics Research Laboratory, Department of Electrical and Computer Engineering, University of Illinois, Urbana, IL

(*Received* 18 *September* 2000; *in final form* 14 *February* 2001)

Abstract—This study characterized the reparative responses in rat lung. Forty-five adult female rats were exposed at two sites over the left lung to 3.1-MHz superthreshold pulsed ultrasound. The repair of lung lesions was evaluated from 0 through 44 days postexposure. Macroscopic lesions at 0 days postexposure were large bright red ellipses of hemorrhage. By 1 and 3 days postexposure, lesions were the same size and dark red to red-black, but, by 3 days postexposure, lesions had a raised surface appearance. From 5 to 10 days postexposure, lesions grew smaller in size, progressed from red-gray to yellow-brown, and retained a raised surface appearance. From 13 through 44 days postexposure, lesions gradually decreased in size, had a faint yellow-brown discoloration, and gradually lost the raised surface appearance. By 37 and 44 days postexposure, lung returned to near normal morphology, but had small areas of light yellow-brown discoloration in the areas where lung was exposed. Microscopic lesions at 0 and 1 days postexposure were areas of acute alveolar hemorrhage. By 3 days postexposure, lesions had loss of alveolar erythrocytes and the formation of hemoglobin crystals. From 5 through 44 days postexposure, iron in degraded erythrocytes was processed to hemosiderin and was negligible in quantity at 44 days postexposure. The proliferation of resident cells (likely alveolar epithelial cells, fibroblasts and endothelial cells) and the infiltration of inflammatory cells in lesions declined in intensity as the lesions aged and was minimal by 44 days postexposure. Under the superthreshold exposure conditions described, lesions induced by ultrasound do not seem to have long-term residual effects in lung. (E-mail: zacharyj@staff.uiuc.edu) © **2001 World Federation for Ultrasound in Medicine & Biology.**

Key Words: **Bioeffects, Healing, Hemorrhage, Lung, Mechanical bioeffects, Nonthermal mechanisms, Pathology, Reparative responses, Ultrasound.**

INTRODUCTION

Pulsed ultrasound is one of the most widely used and safest imaging modalities available in medical practice. Concerns for its safety have recently been raised and addressed by members of the bioeffects research community (American Institute of Ultrasound in Medicine 2000). These concerns are the result of publications describing lung hemorrhage induced in neonatal, juvenile and mature mice (Child et al. 1990; Dalecki et al. 1997b; Frizzell et al. 1994; O'Brien and Zachary 1997; Raeman et al. 1993), mature rats (Holland et al. 1996), mature rabbits (O'Brien and Zachary 1997), 1-day-old and 10-day-old pigs (Baggs et al. 1996; Dalecki et al. 1997a) and infant and mature monkeys (Tarantal and Canfield 1994) at exposure conditions similar to those used for scanning in humans.

Although the pathogenesis of ultrasound-induced lung hemorrhage is unknown, recent studies have suggested that inertial cavitation is not involved in tissue injury (O'Brien et al. 2000). The results of this inertial cavitation study suggest that other mechanical phenomena, such as those associated with radiation force effects, are likely involved in ultrasound-induced lung hemorrhage.

The purpose of this study was macroscopically and microscopically to: (1) characterize the reparative responses of rat lung following superthreshold exposure to pulsed ultrasound; (2) document the time required for repair following exposure; and (3) determine the long-

Address correspondence to: Professor James F. Zachary, University of Illinois, Department of Veterinary Pathobiology, 2001 South Lincoln Avenue, Urbana, IL 61802, USA. E-mail: zacharyj@staff.uiuc.edu

term residual effects of pulsed ultrasound, if any, on lung. The superthreshold exposure value was based on previous studies (O'Brien et al., 2001; Zachary et al., 2001), *i.e.*, exposure levels known to produce lung hemorrhage.

MATERIALS AND METHODS

Exposimetry

Exposure conditions and calibration procedures used in this study have been described previously (O'Brien et al., 2001; Teotico et al., 2001; Zachary et al., 2001). In summary, ultrasonic exposures were conducted using a focused 51-mm-diameter, lithium niobate ultrasonic transducer (Valpey Fisher, Hopkinton, MA, USA) at a center frequency of 3.14-MHz, pulse repetition frequency of 1700-Hz, pulse duration of 1.4-μs, and exposure duration of 60 s. Other water-based pulse-echo transducer characteristics included: fractional bandwidth of 15%, focal length of 56 mm, −6-dB focal beamwidth of 610 μm, and −6-dB depth of focus of 5.9 mm. Calibrations were performed using an automated procedure with a PVDF calibrated hydrophone (Marconi Model Y-34 to 6543, Chelmsford, UK). The *in situ* peak rarefactional pressure at the pleural surface was 17.0 MPa and the *in situ* peak compressional pressure was 39.7 MPa. The *in situ* pressure values were estimated from a measured *in vitro* peak rarefactional pressure of 20.1 MPa (SD = 1.0 MPa, n = 14), a measured *in vitro* peak compressional pressure of 45.7 MPa (SD = 2.8 MPa, n = 14), an intercostal tissue attenuation coefficient of 2.9 dB/cm at 3.14-MHz, and a chest wall thickness of 4.26 mm (SD = 0.39 mm, n = 45). For comparison to a quantity that appears on the display of diagnostic ultrasound equipment, the mechanical index was 5.7. The MI was determined by previously described methodology (Zachary et al., 2001) according to established procedures (ODS, 1998). We recognized that the MI of 5.7 was considerably greater than the regulatory limit of 1.9 (FDA, 1997). The intent of this superthreshold exposure level was to produce lung hemorrhage to evaluate the reparative responses. The exposure level was based on previous studies (O'Brien et al., 2001; Zachary et al., 2001).

Animals

The experimental protocol was approved by the campus' Laboratory Animal Care Advisory Committee and satisfied all campus and NIH rules for the humane use of laboratory animals. Animals were housed in an AAALAC-approved animal facility, placed in groups of three or four in polycarbonate cages with β-chip bedding and wire bar lids, and provided food and water *ad lib.*

Forty-five 10- to 11-week-old female (249 ± 3 g) Sprague-Dawley rats (Harlan, Indianapolis, IN, USA) were exposed to pulsed ultrasound at exposure conditions described under exposimetry. Rats were weighed and anesthetized with ketamine hydrochloride (87.0 mg/kg) and xylazine (13.0 mg/kg) administered IP. The skin of the left thorax was exposed by removing the hair with an electric clipper, followed by a depilatory agent (Nair, Carter-Wallace, Inc., New York, NY, USA) to maximize sound transmission. Two black dots were placed on the skin at approximately the sixth and ninth intercostal spaces to guide the positioning of the ultrasonic beam. Anesthetized rats were placed in right lateral recumbancy and a stand-off tank was positioned in contact with the skin (Fig. 1). The transducer, placed in the stand-off tank that contained degassed water at 30°C, was aligned with the first black dot. The low-power (*in vitro* peak rarefactional pressure of 0.4 MPa, *in vitro* peak compressional pressure of 0.4 MPa, pulse repetition frequency of 10-Hz) pulse-echo capability of the exposure system (RAM5000, Ritec, Inc., Warwick, RI, USA) displayed on an oscilloscope was used to adjust the axial center of the focal region to within 1 mm of the lung surface. Thus, the ultrasonic beam was approximately perpendicular to the skin at the position of the black dot with the beam's focal region at the lateral surface of the lung. The rat was exposed and the procedure was repeated over the second black dot. Three rats were killed at 0 days postexposure by cervical dislocation while under anesthesia immediately following exposure. The remaining 42 rats were allowed to recover from anesthesia. On 1, 3, 5, 7, 10, 13, 16, 19, 23, 27, 30, 34, 37 and 44 days postultrasound exposure, three rats were anesthetized as previously described and killed by cervical dislocation. The elliptical dimensions of lung lesions at the visceral pleural surface were measured immediately after death with a digital micrometer (accuracy: 10 μm), where "a" was the length of the semimajor axis and "b" was the length of the semiminor axis. The lesions were then fixed by immersion in 10% neutral-buffered formalin for a minimum of 24 h. After fixation, lesions were bisected and the depth "d" of the lesion within the lung was measured. In animals where the depth of the lesion was not visually discernible, the depth was determined from measurements made on histologic sections with a slide micrometer. The surface area (πab) and volume (πabd/3) of the lesion were calculated for each animal. Each half of the bisected lesion was embedded in paraffin, sectioned at 5 μm, stained with hematoxylin and eosin, and evaluated microscopically.

Data analyses

Data analyses included calculation of surface area and volume and the macroscopic and microscopic characterization of lung lesions at each time point. Summary

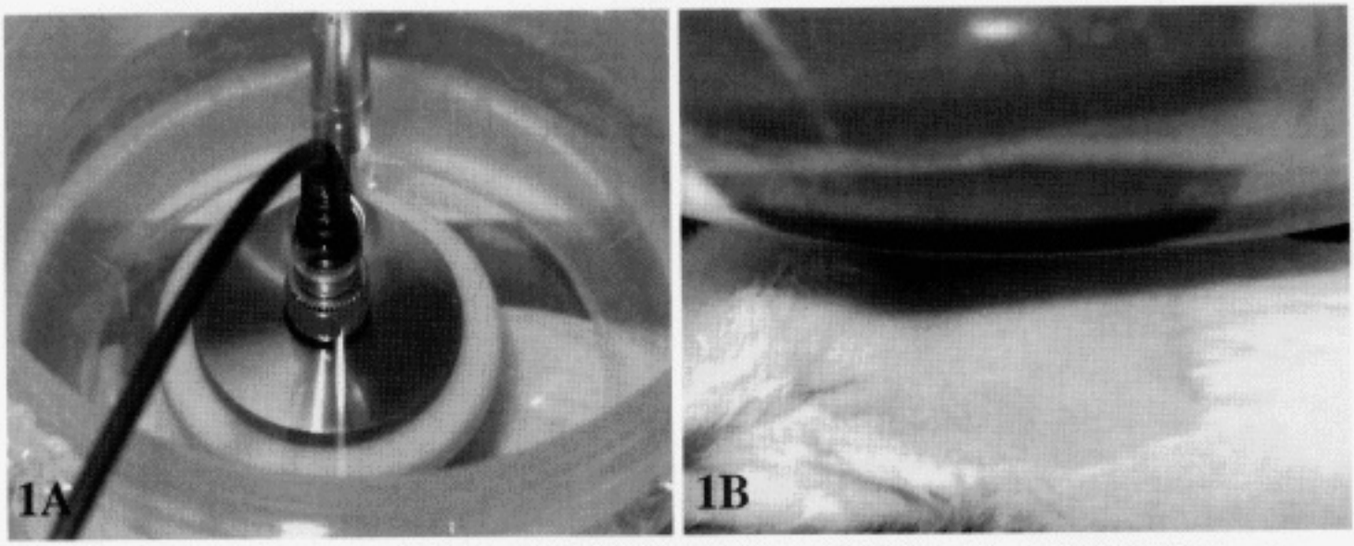

Fig. 1. (A) Rats were exposed for 60-s duration to pulsed ultrasound in right lateral recumbency using a focused 51-mm-diameter, lithium niobate ultrasonic transducer (back side of transducer shown) at a center frequency of 3.14-MHz, pulse repetition frequency of 1700-Hz, and pulse duration of 1.4-μs. (B) The membrane of the stand-off vessel made direct contact with the skin surface. A small quantity of ultrasonography gel was used to ensure complete contact between the membrane and the skin. The *in situ* peak rarefactional pressure at the pleural surface was 17.0 MPa; the *in situ* peak compressional pressure was 39.7 MPa.

statistics for each time point included means of group measurements and plots of the means of lesion surface area, depth and volume vs. days postexposure. Means and standard errors of the means (SEMs) for lesion measurements were based on six lesions ($n = 6$) per postexposure group, that is, three rats per group and two lesions per rat. In four of the 15 postexposure groups (days 7, 10, 13 and 23), one of the three rats in a group had only one lesion on the left lung lobe and therefore five lesions were used for measurements. For these four groups, means and SEMs for lesion measurements were based on five lesions ($n = 5$) per postexposure group.

RESULTS

Macroscopic characterization of lung lesions

The notable macroscopic characteristics of lesions in lung at each day postexposure are listed in Table 1 and illustrated in Fig. 2. In summary, following exposure to pulsed ultrasound, the lesions at 0 days postexposure were bright red to red elliptical areas of acute hemorrhage under the visceral pleural surface. The lesion had a darker central area of severe hemorrhage that likely was centered at the focus of the beam. This area was surrounded by a prominent rim of less intense hemorrhage. The hemorrhage extended into subjacent parenchyma to form a conical shape. The base of the cone was at the pleural surface and the apex was within the lung parenchyma at the deepest extent of the lesion. From 1 day postexposure through 7 days postexposure, lesions retained a similar overall shape but had a gradual reduction in surface area, depth and hence, volume, as well as an overall color change that progressed from red to dark red to brown-yellow (Figs. 2 and 3). From 10 days postexposure through 44 days postexposure, lesions retained a

Table 1. Macroscopic characteristics of lesions versus time following superthreshold exposure to pulsed ultrasound

Days postexposure	Tissue response
0	Bright red to red elliptical areas of acute hemorrhage under the visceral pleural surface with extension of the lesion into subjacent parenchyma to form a conical shape. The base of the cone is at the pleural surface; the apex is within lung parenchyma.
1	Red to dark red elliptical areas of hemorrhage. Lesion area, depth and volume are essentially unchanged.
3	Dark red to black elliptical areas of hemorrhage. Lesion area, depth and volume are essentially unchanged. Lesions have a raised surface appearance.
5	Gray to brown elliptical areas of resolving hemorrhage. Lesions have a raised pale center. Lesion area, depth and volume have decreased.
7	Brown to yellow-brown elliptical areas of resolving hemorrhage. Lesions have a raised pale center. Lesion area, depth and volume have decreased.
10–44	Yellow-brown elliptical areas of hemorrhage that progressively decrease in size to small yellow-tan foci. Lesions have a raised pale center that decrease in magnitude with time to a normal surface contour. Lesion characteristics, area, depth and volume decrease over time.

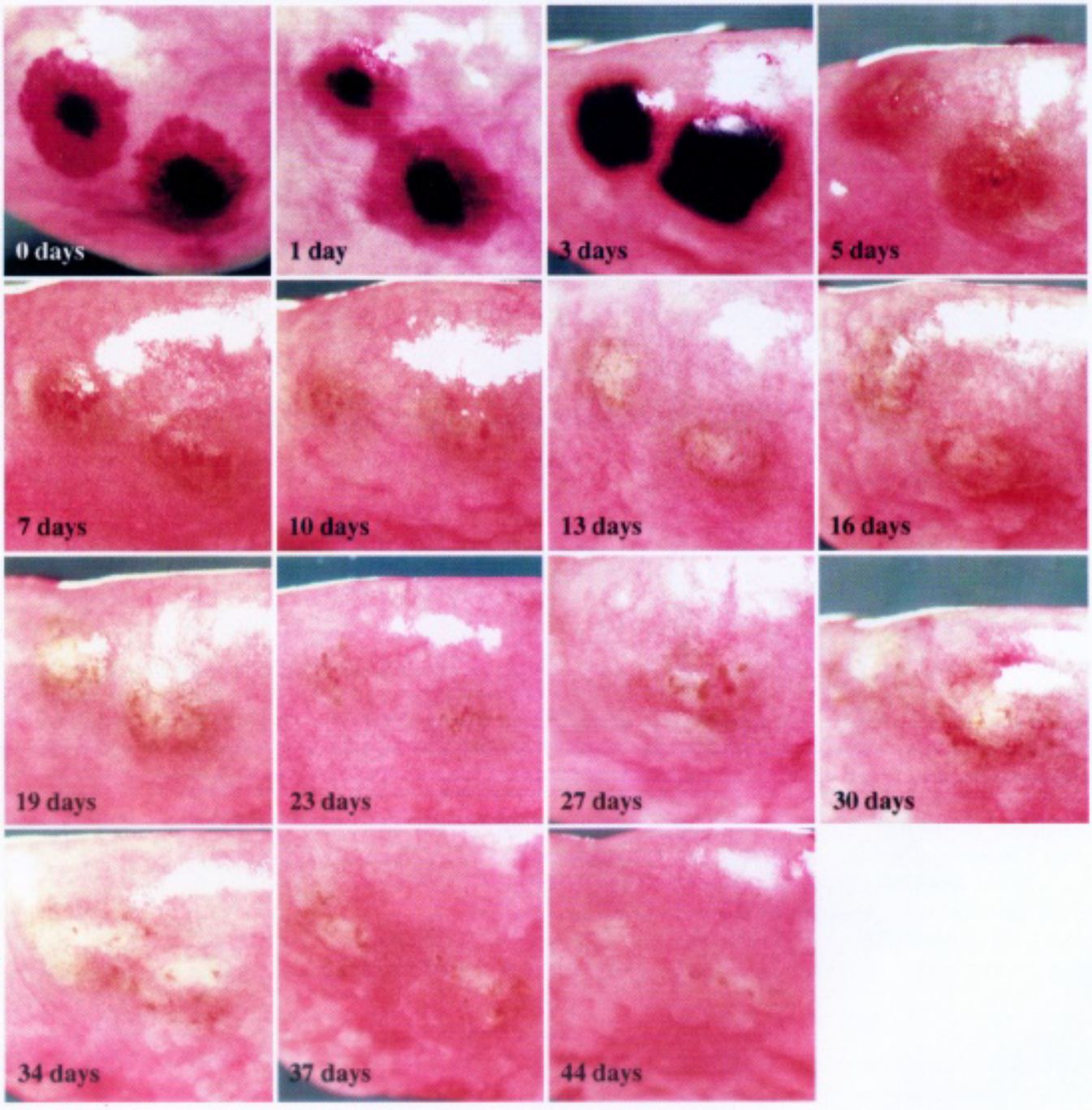

Fig. 2. Macroscopic lesions induced in lung following exposure to ultrasound under the conditions described in Fig. 1. The acute hemorrhage (bright red ellipses) present on 0 days postexposure is gradually repaired and returned to near normal by 44 days postexposure. Photomicrographs of each lesion time point should be correlated with lesion descriptions provided in Table 1.

similar overall shape, but had a gradual and continual reduction in lesion surface area, depth and volume. In addition, during this time period, lesions changed in color from brown-yellow to light yellow, a reflection of the removal of hemosiderin pigment from the lesion and the resolution of the hemorrhage (Fig. 2).

From 3 days postexposure through 19 days postexposure, the surface of the lesions was raised and lighter in color than the surrounding injured area. From 23 days postexposure through 44 days postexposure, the raised appearance of the surface gradually diminished and the lung surface contour returned to normal.

Microscopic characterization of lung lesions

The notable microscopic characteristics of lesions in lung at each day postexposure are listed in Table 2 and

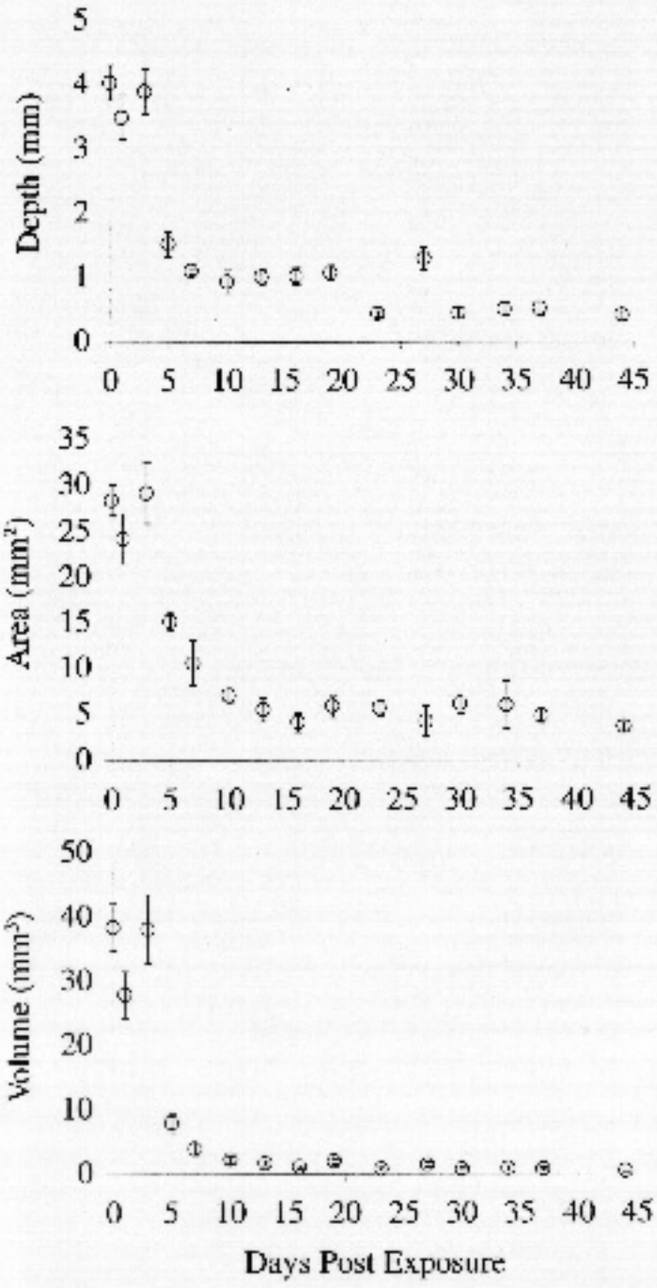

Fig. 3. Quantitative changes in lesion depth, surface area and volume following exposure to pulsed ultrasound. Each symbol represents the mean of six lesions ($n = 6$) per postexposure group with the exception of four postexposure groups (days 7, 10, 13 and 23). For these four groups, each symbol represents the mean of five lesions ($n = 5$) per postexposure group. Error bars represent standard error of the means ($n = 5$ or 6).

Table 2. Microscopic characteristics of lesions versus time following superthreshold exposure to pulsed ultrasound

Days postexposure	Tissue response
0	Acute alveolar hemorrhage without pleural or septal injury.
1	Acute alveolar hemorrhage without pleural or septal injury. Early phases of proliferative cellular and eosinophilic leukocyte inflammatory cell responses begin. The initial proliferative phase consists of hypertrophy and hyperplasia of cells lining alveolar septa.
3	Alveolar hemorrhage with erythrocyte degradation and hemoglobin crystal formation. Proliferative cellular and eosinophilic leukocyte inflammatory cell responses increase in magnitude. The proliferative phase consists of hypertrophy and hyperplasia of epithelial and mesenchymal cells comprising alveolar septa.
5	Alveolar hemorrhage with erythrocyte degradation and hemoglobin crystal formation. Proliferative cellular and eosinophilic inflammatory responses increase in magnitude.
7–10	Erythrocyte degradation, hemoglobin crystal formation, and hemosiderial pigment accumulation continue. Proliferative cellular and eosinophilic leukocyte inflammatory cell responses continue.
13	Erythrocyte degradation almost completed, hemoglobin crystal formation prominent, and hemosiderin pigment accumulation prominent. Proliferative cellular and eosinophilic inflammatory responses begin to resolve.
16	Erythrocyte degradation complete, hemoglobin crystal formation prominent, and hemosiderin pigment accumulation prominent. Proliferative cellular and eosinophilic inflammatory responses continue to resolve.
19–44	Erythrocyte degradation complete, hemoglobin crystal formation prominent, and hemosiderin pigment accumulation prominent. Proliferative cellular and eosinophilic inflammatory responses gradually subside and are minimal; alveolar architecture has returned to normal. By 44 days postexposure, essentially normal lung parenchyma with minimal septal fibrosis and hemosiderosis.

illustrated in Figs. 4 and 5. In summary, following exposure to pulsed ultrasound, the lesions at 0 days postexposure were characterized by areas of acute alveolar hemorrhage under the visceral pleural surface without pleural or septal injury. From 1 day postexposure through 10 days postexposure, the lesions exhibited progressive stages of erythrocyte degradation, the accumulation of hemoglobin pigment crystals and the production of variable quantities of a brown to yellow pigment (hemosiderin). Beginning at 1 day postexposure and continuing through 16 days postexposure, a proliferative cellular reparative response was also observed. This response consisted of the proliferation of large numbers of epithelial and mesenchymal cells in the exposed area that altered the normal alveolar architecture (Fig. 4, see 1 through 16 days postexposure and Fig. 5, see 1 through 7 days postexposure). The phenotype(s) of these cells could not be adequately determined by light microscopy with routine histochemical staining, but likely include type II alveolar epithelial cells, alveolar macrophages, smooth muscle cells of vascular origin and fibroblasts. The phenotype(s) of these cells will be evaluated further

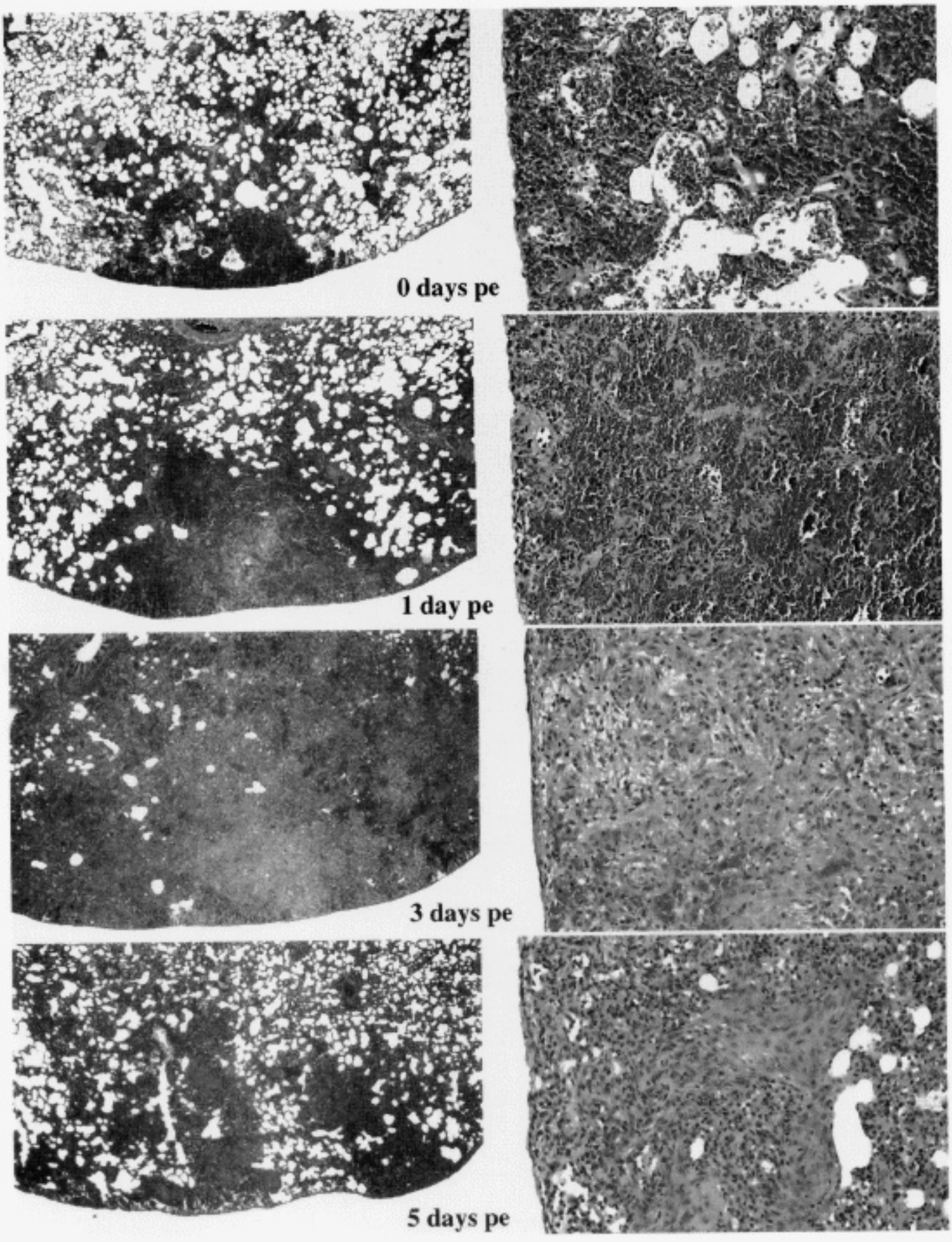

Fig. 4. (continued)

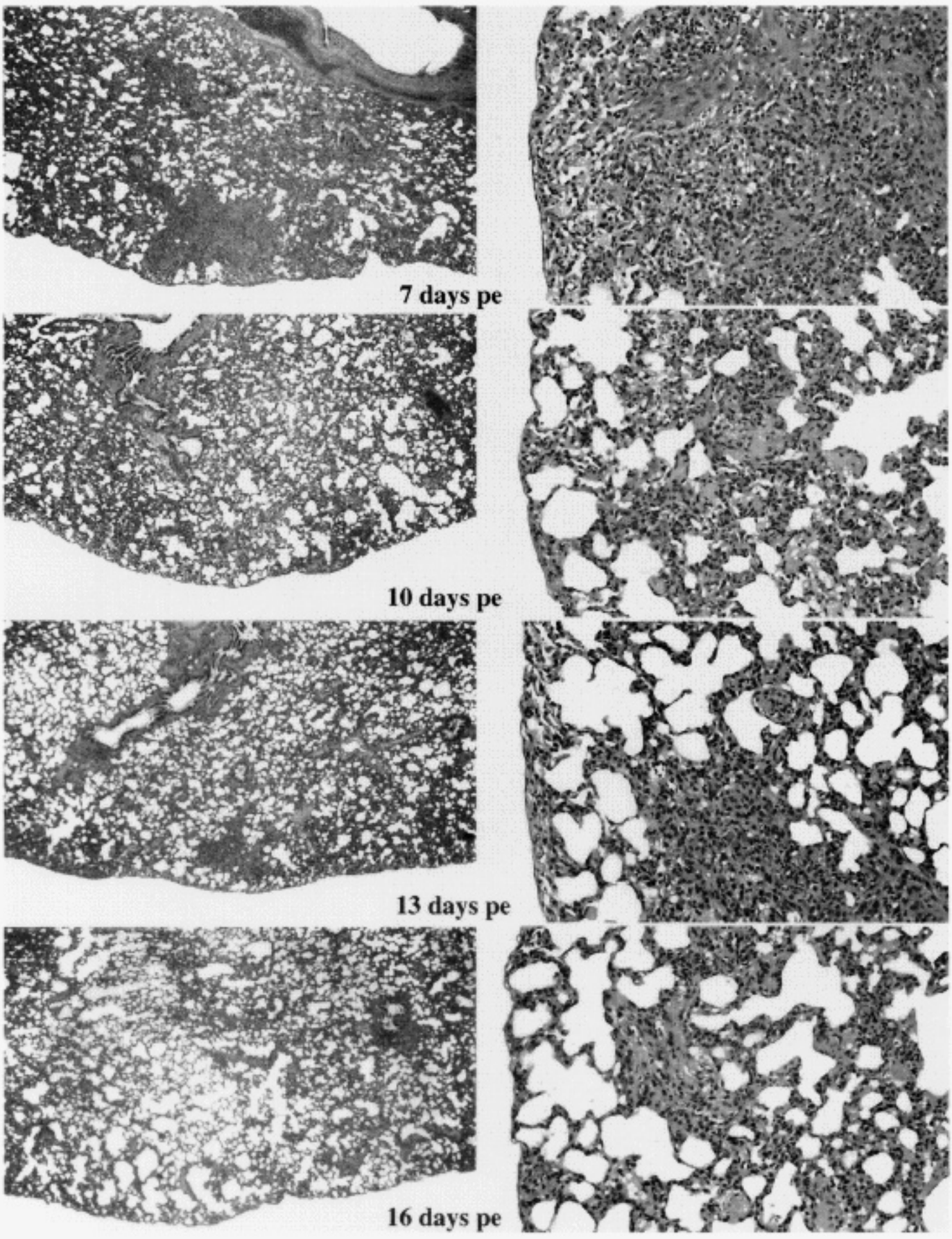

Fig. 4. (continued).

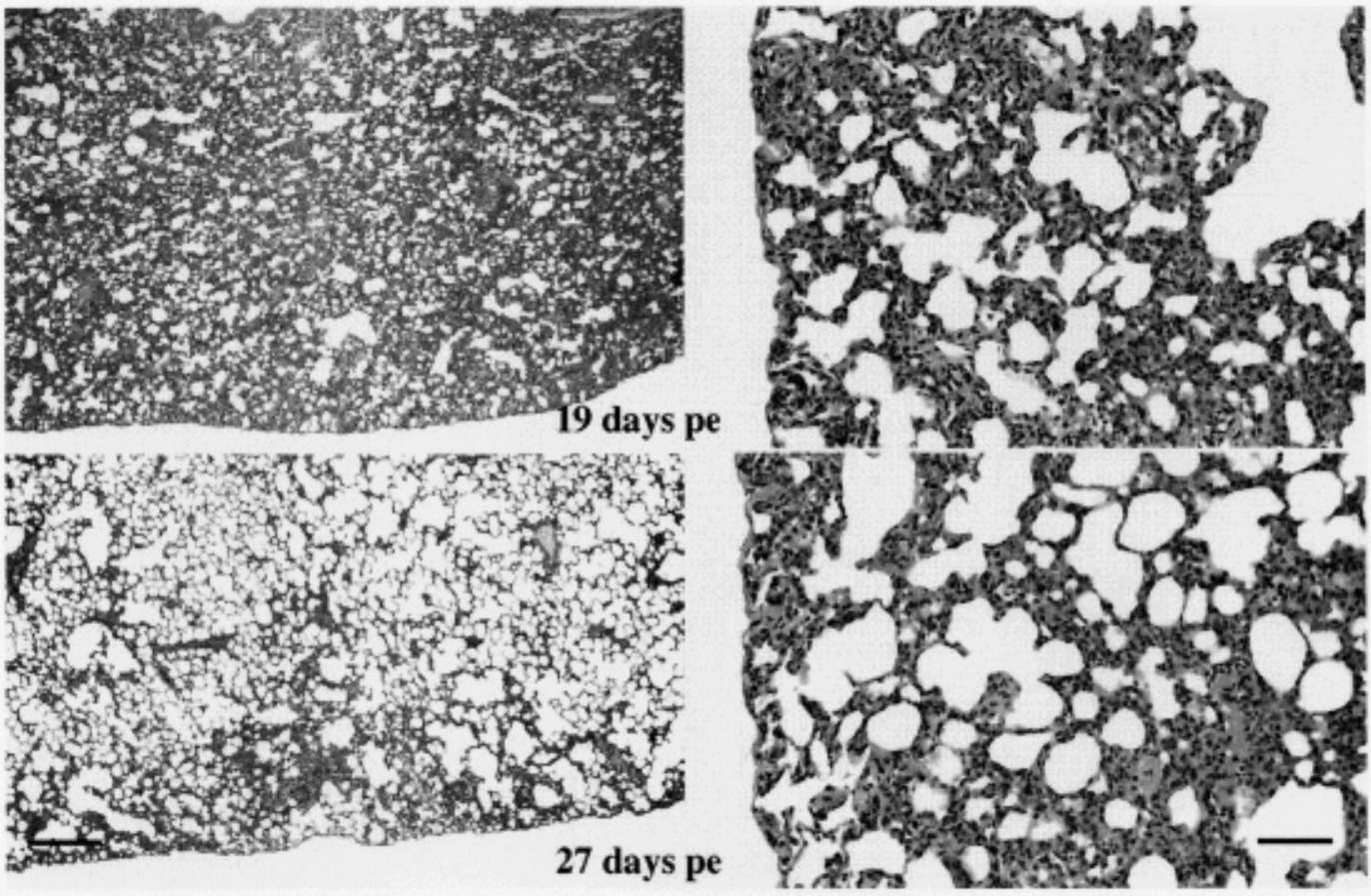

Fig. 4. Microscopic lesions induced in lung following exposure to ultrasound under the conditions described in Fig. 1. Photomicrographs of lesions are paired for each time point to demonstrate the overall lesion appearance at low (extent of fully aerated alveoli) and medium (specific cellular proliferative responses) magnifications. Photomicrographs should be correlated with lesion descriptions provided in Table 2. The acute hemorrhage present on 0 days postexposure is gradually removed and repaired by a proliferative cellular response (1 through 16 days postexposure) that is nearly resolved by 44 days postexposure. Lesions from 30 to 44 days postexposure are similar too, but less severe than the lesion illustrated in the photomicrograph for 27 days postexposure. H&E stain. Scale bar for the entire left panel (lower magnification) is present in the photomicrograph of 27 days postexposure (bar = 400 μm; left panel). Scale bar for the entire right panel (higher magnification) is present in the photomicrograph of 27 days postexposure (bar = 80 μm; right panel).

and reported in a future publication. The reparative response was also accompanied by an inflammatory exudate comprised of eosinophils admixed with lesser numbers of lymphocytes and monocytes. The inflammatory response was noted at 1 day postexposure and was resolved by 19 days postexposure.

From 1 day postexposure through 10 days postexposure, affected alveoli were essentially obliterated by this reparative response, and there was no area for effective air exchange. From 13 days postexposure through 44 days postexposure, the proliferation of cells subsided and, by 44 days postexposure, alveolar architecture of the exposed area had returned to near normal except for small areas of subpleural and septal fibrosis. From 10 through 16 days postexposure, the degradation and removal of hemoglobin pigment resulted in the formation of appreciable quantities of hemosiderin pigment that was deposited in macrophages within lung tissue as a brown to yellow pigment. As the lesion aged, the quantities of this pigment decreased substantially. From 19 through 44 days postexposure, hemoglobin and hemosiderin were processed and removed from the lesions, the inflammatory responses subsided, and septal and alveolar architecture returned to near normal (Fig. 4). By 44 days postexposure, the exposed area had small foci of septal fibrosis that contained hemosiderin pigment within macrophages at the site of ultrasound exposure just under the visceral pleura.

DISCUSSION

Ultrasound-induced lung injury resulted in severe alveolar hemorrhage and a vigorous reparative response. Macroscopically and microscopically, injured tissue re-

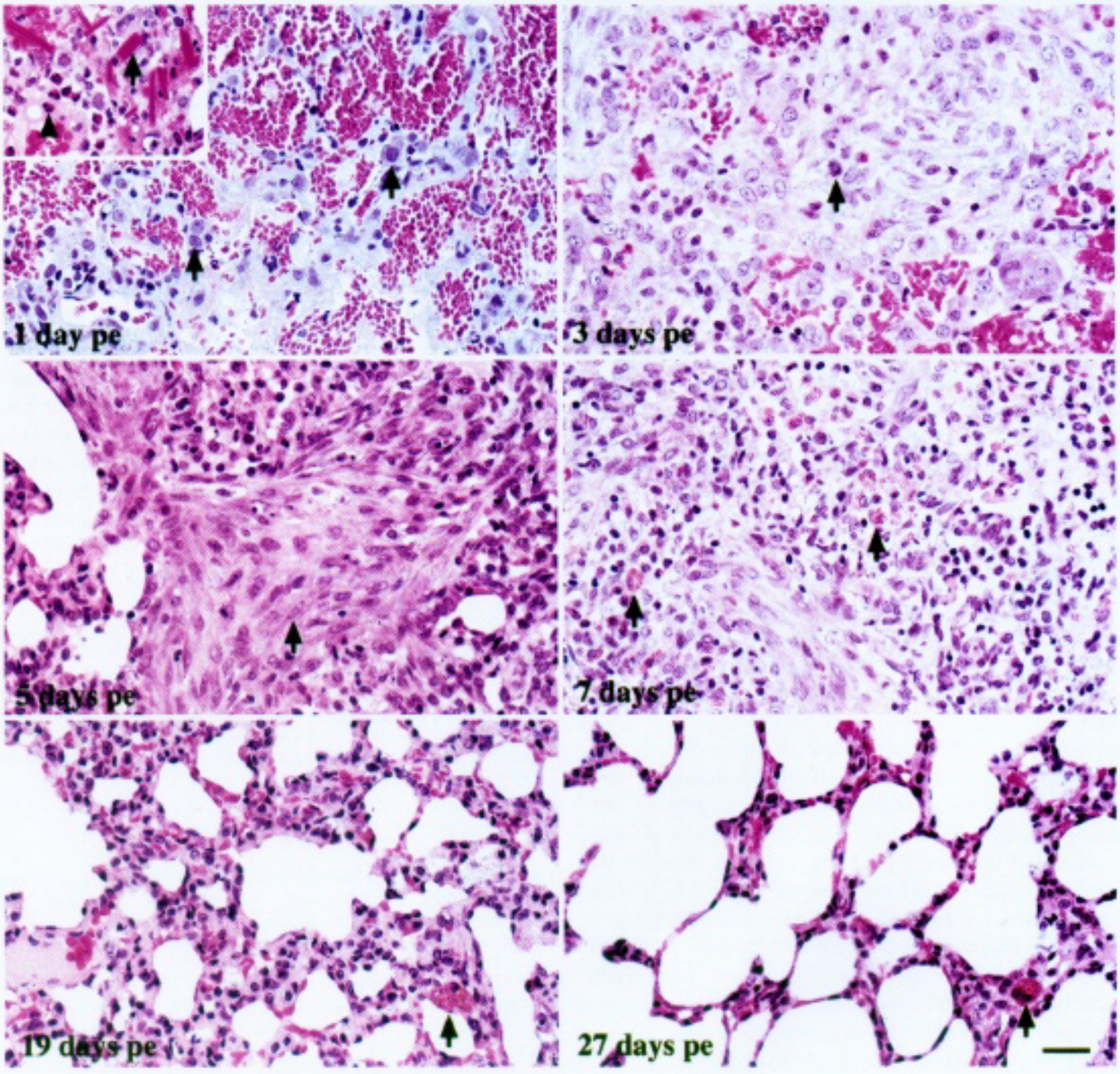

Fig. 5. Characteristics of specific microscopic lesions following exposure to ultrasound under the conditions described in Fig. 1. One day postexposure: early phase of the proliferative response is characterized by hypertrophy of cells associated with alveolar septa (arrows) and alveolar hemorrhage. Inset: acute inflammation dominated by eosinophils (arrowhead) and hemoglobin crystal formation (arrow) were also present in the lesion. Three days postexposure: alveoli are obliterated by a proliferative cellular response that includes cells in mitosis (arrow). The response consists of macrophages and other epithelial and mesenchymal cells. Acute inflammatory cells are also present. Alveolar hemorrhage is being resolved by erythrocyte degradation through phagocytosis by macrophages. Five days postexposure: spindloid cells (arrow) of likely mesenchymal origin (fibroblasts or smooth muscle) form a component of the proliferative response. Acute inflammatory cells are also present. Alveolar hemorrhage is minimal due to phagocytosis. Seven days postexposure: the proliferative and inflammatory responses are still prominent. Processing of phagocytized erythrocytes has resulted in the accumulation of hemosiderin pigment in macrophages (arrows). Nineteen days postexposure: alveolar architecture is returning to normal. The proliferative and inflammatory responses have subsided. Alveoli and alveolar septa are again discernable and hemosiderin pigment is present within macrophages (arrow) in alveolar septa. Twenty-seven days postexposure: alveolar architecture is near normal. The proliferative and inflammatory responses are essentially resolved; however, small areas of septal fibrosis remain. Alveoli and alveolar septa are clearly discernible and near proper size. Hemosiderin pigment is present within macrophages (arrow) in alveolar septa. H&E stain. Scale bar for all figures is present in the photomicrograph of 27 days postexposure (bar = 40 μm).

turned essentially to normal following repair, but there were small foci of fibrosis and hemosiderosis at 44 days postexposure at the site of exposure. Based on morphologic analysis, the reparative response that ensued under the superthreshold exposure conditions described in this study resulted in no substantive long-term residual effects that would be detrimental to normal alveolar function and air exchange. The rapidity and severity of the proliferative response of specific populations of cells within the exposed lung was unexpected. Alveolar macrophages (blood monocytes) would be expected to play an important role in removing and degrading erythrocytes, processing hemoglobin pigment and removing hemosiderin pigment from lung. The proliferation of probable type II alveolar epithelial cells, fibroblasts and other unidentified spindloid cell types was unanticipated, but type II alveolar epithelial cells are the cells in lung that proliferate following other types of toxic, metabolic and infectious injury. The tissue and cellular characteristics of this proliferative response may be related to cytokines or other growth factors associated with the elicited eosinophilic leukocyte inflammatory response. The role of ultrasound and its interaction with resident and recruited inflammatory cells in potentiating inflammatory and proliferative reparative responses warrants further investigation.

A review of the biomedical literature describes lesions in humans following alveolar hemorrhage in a group of diseases classified under the category of "diffuse pulmonary hemorrhage syndromes." These diseases include Goodpasture's syndrome, collagen vascular diseases, and causes of diffuse pulmonary hemorrhage without an immunologic basis (idiopathic pulmonary hemosiderosis) (Capron 1996; Corrin 2000; Miller 1995). In these diseases, alveolar hemorrhage results from injury (autoimmune or unknown causes) to the pulmonary microvasculature. Reparative responses to alveolar hemorrhage include alveolar lining cell hyperplasia (type II), subacute to chronic inflammation, hemosiderosis (free and within macrophages) and varied degrees of alveolar and septal fibrosis. These responses are thought to be a nonspecific reaction to intraalveolar blood. Because most of these human diseases are chronic in nature, alveolar and septal fibrosis can be prominent and unresolvable. The lesions induced by ultrasound in this study appear more proliferative than the lesions described in "diffuse pulmonary hemorrhage syndromes" of humans.

Even although it is apparent that extravascular (intraalveolar) erythrocytes and their degradation byproducts are sufficiently irritating to elicit proliferative cellular responses in the lung, the reaction of lung to alveolar hemorrhage regardless of its cause (ultrasound, immunologic or unknown) suggests that cells within lung have a limited repertoire of responses to injury. Although it is unlikely that ultrasound directly caused the eosinophilic leukocyte inflammatory response or the proliferative reparative response in this study, ultrasound has been shown directly to cause cellular activation (Parvizi et al. 1999; Yang et al. 1966). As a result, the character and phenotype of the cell populations involved in this proliferative response need to be investigated in greater detail .

CONCLUSIONS

Ultrasound-induced lung injury resulted in severe alveolar hemorrhage and a vigorous reparative response. The reparative response that ensued under the exposure conditions described in this study resulted in no substantive long-term residual effects that would be detrimental to normal alveolar function and air exchange. Macroscopically and microscopically, injured lung essentially returned to normal by 44 days postexposure, but had small foci of fibrosis and hemosiderosis. Based on morphologic analysis, it was likely that lung function was also normal.

Acknowledgements—This work was supported, in part, by NIH grant HL58218 awarded to WDO and JFZ. We thank B. Zierfuss, K. Clemens, B. McNeill, R. McQuinn, B. Qiao, J. Sempsrott, and A. Wunderlich from the Bioacoustics Research Laboratory, University of Illinois for technical contributions. We also thank the Histopathology Laboratory, College of Veterinary Medicine for processing and staining the lung lesions.

REFERENCES

American Institute of Ultrasound in Medicine: Mechanical Bioeffects from Diagnostic Ultrasound: AIUM Consenses Statements. J Ultrasound Med 2000;19:67–168.

Baggs R, Penney DP, Cox C, Child SZ, Raeman CH, Dalecki D, Carstensen EL. Thresholds for ultrasonically induced lung hemorrhage in neonatal swine. Ultrasound Med Biol 1996;22:119–128.

Capron F. Pulmonary hemorrhage syndromes. In: Hasleton PS, ed. Spencer's pathology of the lung. New York: McGraw-Hill, 1996: 865–874.

Child SZ, Hartman CL, Schery LA, Carstensen EL. Lung damage from exposure to pulsed ultrasound. Ultrasound Med Biol 1990;16:817–825.

Corrin B. Pathology of the lungs. London: Churchill Livingstone, 2000:401–405.

Dalecki D, Child SZ, Raeman CH, Cox C, Carstensen EL. Ultrasonically induced lung hemorrhage in young swine. Ultrasound Med Biol 1997a;23:777–781.

Dalecki D, Child SZ, Raeman CH, Raeman CH, Cox C, Penney DP, Carstensen EL. Age dependence of ultrasonically-induced lung hemorrhage in mice. Ultrasound Med Biol 1997b;23:767–776.

FDA, Information for Manufacturers Seeking Marketing Clearance of Diagnostic Ultrasound Systems, and Transducers. Center for Devices, and Radiological Health, US Food, and Drug Administration, Rockville, MD, September 30, 1997.

Frizzell LA, Chen E, Lee C. Effects of pulsed ultrasound on the mouse neonate: Hind limb paralysis and lung hemorrhage. Ultrasound Med Biol 1994;20:53–63.

Holland CK, Deng CX, Apfel RE, Alderman JL, Fenandez LA, Taylor KJW. Direct evidence of cavitation *in vivo* from diagnostic ultrasound. Ultrasound Med Biol 1996;22:917–925.

Miller RR. Diffuse pulmonary hemorrhage. In: Thurlbeck WM, Churg

AM, eds. Pathology of the lung. New York: Thieme Medical Publishers, 1995:349–374.

O'Brien WD Jr, Zachary JF. Lung damage assessment from exposure to pulsed-wave ultrasound in the rabbit, mouse, and pig. IEEE T Ultrason Ferr 1997;44:473–485.

O'Brien WD Jr, Frizzell LA, Weigel RM, Zachary JF. Ultrasound-induced lung hemorrhage is not caused by inertial cavitation. J Acoust Soc Am 2000;108:1290–1297.

O'Brien WD Jr, Frizzell LA, Schaeffer DJ, Zachary JF. Superthreshold behavior of ultrasound-induced lung hemorrhage in adult mice and rats: Role of pulse repetition frequency and exposure duration. Ultrasound Med Biol, 2001;27:267–277.

ODS, Standard for Real-Time Display of Thermal, and Mechanical Acoustic Output Indices on Diagnostic Ultrasound Equipment, Rev. 1. Am Institute of Ultrasound in Medicine, Laurel, MD, and National Electrical Manufacturers Association, Rosslyn, VA, 1998.

Parvizi J, Wu CC, Lewallen DG, Greenleaf JF, Bolander ME. Low-intensity ultrasound stimulates proteoglycan synthesis in rat chondrocytes by increasing aggrecan gene expression. J Orthop Res 1999;17:488–494.

Raeman CH, Child SZ, Carstensen EL. Timing of exposures in ultrasonic hemorrhage of murine lung. Ultrasound Med Biol 1993;19: 507–512.

Raeman CH, Child SZ, Dalecki D, Cox C, Carstensen EL. Exposure-time dependence of the threshold for ultrasonically induced murine lung hemorrhage. Ultrasound Med Biol 1996;22:139–141.

Tarantal AF, Canfield DR. Ultrasound-induced lung hemorrhage in the monkey. Ultrasound Med Biol 1994;20:65–72.

Teotico GA, Miller RJ, Frizzell LA, Zachary JF, O'Brien WD Jr. Attenuation coefficient estimates of mouse and rat chest wall. IEEE T Ultrason Ferr 2001;48:593–601.

Tyler WS, Julian MD. Gross and subgross anatomy of lungs, pleura, connective tissue septa, distal airways, and structural units. In: Parent RA, ed. Comparative biology of the normal lung. Boca Raton, FL: CRC Press, 1992:37–47.

Yang KH, Parvizi J, Wang SJ, Lewallen DG, Kinnick RR, Greenleaf JF, Bolander ME. Exposure to low-intensity ultrasound increases aggrecan gene expression in a rat femur fracture model. J Orthop Res 1996;14:802–809.

Zachary JF, O'Brien WD Jr. Lung lesion induced by continuous- and pulsed-wave (diagnostic) ultrasound in mice, rabbits, and pigs. Vet Pathol 1995;32:43–45.

Zachary JF, Sempsrott JM, Frizzell LA, Simpson DG, O'Brien WD Jr. Superthreshold behavior and threshold estimation of ultrasound-induced lung hemorrhage in adult mice and rats. IEEE T Ultrason Ferr 2001;48:581–592.